Methods for surface roughness elimination from thermal-wave frequency scans in thermally inhomogeneous solids

Lena Nicolaides and Andreas Mandelis[a)]
Photothermal and Optoelectronic Diagnostics Laboratories, Department of Mechanical and Industrial Engineering, University of Toronto, 5 King's College Road, Toronto, Ontario, M5S 3G8 Canada

[(Received 8 January 2001; accepted for publication 14 May 2001)

Two approaches for eliminating surface roughness in the thermal-wave frequency response of inhomogeneous solids are developed. The first approach is based on the theoretical formulation of roughness as an effective homogeneous overlayer and is adequate for eliminating low roughness levels from experimental data. The second approach models roughness as random spatial white noise resulting in a linear superposition of logarithmic-Gaussian distributions representing roughness scales in the spatial frequency spectrum and in the modulation frequency domain. Two scales of roughness on the surface of hardened AISI 8620 steel with the same hardness depth profiles are found and the experimental data are reconstructed to retrieve similar inhomogeneous thermal diffusivity depth profiles. © *2001 American Institute of Physics.*
[DOI: 10.1063/1.1383579]

I. INTRODUCTION

Modeling roughness is a nontrivial problem. In most photothermal applications, the surface of the sample is polished so that roughness effects can be neglected. Besides its own inherent merit in revealing underlying structures, a method of ''eliminating'' roughness mathematically can also be advantageous for practical applications. Roughness effects on the photothermal signal were reported as early as 1986–87 by Bein *et al.*[1] Those authors have modeled roughness as a three-layer model and have found that the rough surface has a low thermal effusivity, the intermediate porous layer has an increased thermal effusivity and, finally, the bulk has the highest thermal effusivity. Thermal diffusion through the random distribution of spatial roughness can be modeled using fractal analysis in the micrometer or submicrometer scale. Osiander *et al.*[2] studied the influence of a random sample structure on the transport of heat using the concept of fractals as introduced into the thermal-wave field by Alexander and Orbach in 1982.[3] These authors applied the concept of the fracton, or spectral dimension, to describe diffusion processes in fractals. Boccara and Fournier[4] further introduced fractals on randomly structured samples to measure time dependence of thermal diffusion that deviates appreciably from Euclidean behavior. Vandembroucq and Roux[5] developed a methodology based on conformal mappings to account for the random geometry of the surface to which boundary conditions are applied. Both harmonic[5] and biharmonic[5] problems were treated and the authors discussed the possibility of using the method in diffusion and wave propagation problems. Vandembroucq and Boccara[5] applied the concept of conformal mapping in obtaining the local temperature field of a rough surface heated with a modulated focused laser beam.

In photothermal signals roughness appears at high frequencies, manifesting itself as a broad peak in the phase (and possibly in the amplitude) data, affecting the signal well beyond the roughness depth and making it necessary to account for. The above methods concentrated on modeling and understanding heat diffusion through surface roughness of homogeneous solids. The purpose of this work is not only a generalization in the form of modeling roughness in inhomogeneous solids, but also to eliminate the component of the signal associated with it, so that the underlying thermophysical profiles of the investigated material can be obtained. Two approaches of modeling roughness are presented. The first approach treats roughness as a homogeneous finite layer over a semi-infinite inhomogeneous layer. With this method the inhomogeneous layer is reconstructed beyond the roughness mean depth. With a low-level roughness, the results are satisfactory but this theoretical model, however, proves to be too simplistic. As the spatial dimensions of roughness increase, the thermal wave spectrum becomes more complicated, with the effects of roughness extending farther into the low-frequency range, potentially resulting in the reconstruction of erroneous thermal diffusivity profiles. Therefore, a second approach is introduced, based on regarding roughness as a random process in the experimental data. The effects of inhomogeneity and roughness can then be deconvoluted from the total signal. The method is implemented to reconstruct thermal-diffusivity depth profiles from two identically carburized steel samples with different roughness scales on their surfaces.

II. MATERIALS AND RESULTS

Thermal-wave depth profilometry is most conveniently dealt with theoretically as a one-dimensional problem and therefore the experimental setup must have a low lateral spatial resolution. In our experiments we chose to use conventional frequency-domain laser infrared photothermal radiom-

a)Electronic mail: mandelis@mie.toronto.ca

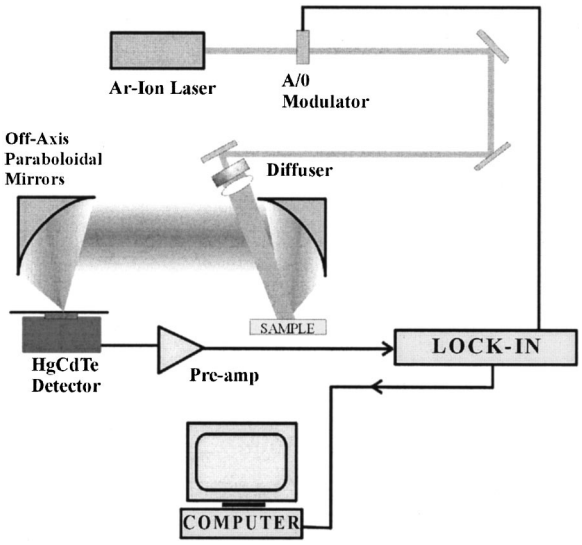

FIG. 1. Frequency-domain photothermal radiometric instrumentation for roughness elimination and thermal-wave depth profilometry.

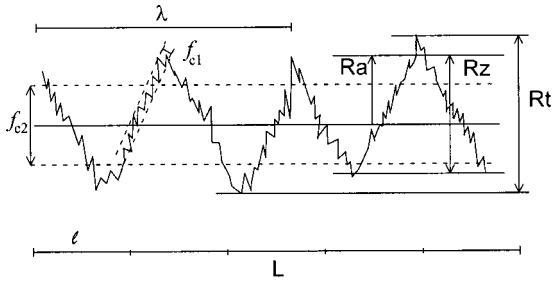

FIG. 2. Two levels of roughness centered at characteristic frequencies f_{cl} (high) and f_{c2} (low).

etry (PTR) as the thermal-wave probe technique. To maintain the one-dimensional heat diffusion formalism assumed in the theory, the pump beam spot size was made much larger than the maximum profile depth. In addition to the spotsize another important consideration is the beam shape. Typical TEM_{00}-mode laser sources have a Gaussian profile, and what is needed ideally is a top-hat intensity distribution. To alleviate these problems a thick diffuser with a lens was placed in the path of our beam for broadening it and reducing its Gaussian profile. Three dimensionality effects in the depth profilometry of steels were, as expected, more pronounced at low frequencies, typically below 10 Hz. The experimental PTR apparatus has been described elsewhere[6] and is shown in Fig. 1.

A major part of this work is centered on the effect of roughness on reconstructed thermal-diffusivity depth profiles, since thermal-wave signal frequency responses are influenced to variable extents by surface roughness. The samples used were 1 cm thick (thermally semi-infinite), and were cut from the same slab of AISI 8620 steel alloy, which is a low carbon steel (0.25%C). The surface roughness of the samples was controlled with a 200 and 600 grit silicon carbide (SiC) grinding paper. The mean roughness thickness *d* of each sample was measured independently with a surfometer (Series 400; Precision Devices, Milan, MI) with a 0.01 μm total system resolution. The surface profile parameters are explained below and are illustrated in Fig. 2. The evaluation length *L* (the length over which the surface parameters are evaluated $L=10$ mm) for each measurement consisted of five sampling lengths. The sampling length *l* is defined as the nominal spatial wavelength used for separating roughness and waviness λ. Roughness includes the finest (shortest wavelength) irregularities of a surface and waviness includes the more widely spaced (longer wavelength) deviations of a surface from its nominal shape. For each measurement the following three surface parameters were documented: (1) roughness average *Ra*; (2) maximum height of the profile *Rt*; and (3) average maximum height of the profile *Rz*. *Ra* is the arithmetic average of the absolute values of the profile heights over the evaluation length. *Rt* is the vertical distance between the highest and lowest points of the profile within the evaluation length. *Rz* is the average of the successive values of Rt_i (*Rt* of the *i*th sampling length) calculated over the evaluation length. The measurements were repeated at three independent positions on the surface of the sample, and the final value of each surface parameter was obtained as an average of the three measurements. The average of the three independent *Rz* values $\mathrm{avg}_3(Rz)$ was used as the mean roughness thickness *d*. This parameter was chosen as the effective thickness that generates the photothermal signal that can be modeled as a homogenous layer on a semi-infinite substrate.

The roughness thickness *d* of the 200 and 600 grit samples was measured to be 5 and 2.5 μm, respectively. Sequential experimental frequency scans in the range of 0.5 Hz–100 kHz were performed on the samples. The experimental surface temperature response on the sample was normalized by the surface temperature response of a reference sample (Zr alloy). This gave, for each frequency, an amplitude ratio and a phase difference. The normalizing procedure was necessary to correct all instrumental frequency dependencies. Roughness manifests itself most strongly at high frequencies and Fig. 3 shows the normalized responses of two homogeneous AISI 8620 steel samples with 200 and 600 grit roughness. The roughest surface shows a peak in the phase data which affects the signal beyond the expected roughness depth and strongly deviates from the theory of a homogeneous sample. The signal response from the smaller roughness sample is less influenced at low frequencies where it resembles the flat behavior for a normalized homogeneous sample.

The two AISI 8620 samples with 200 and 600 grit roughness were then carburized at 0.02 in. depth. Carburizing is the process by which the carbon concentration of a ferrous alloy is increased by diffusion. In this heat treatment, pearlite formation is accomplished by carbon diffusion. Figure 4 shows the experimental response of the two carburized samples. Above 1000 Hz strong effects due to roughness are observed. The roughness thickness of the samples after carburization was remeasured with the surfometer and was found to be approximately the same as before, within a tolerance of ± 0.1 μm. Thus, any change from the untreated high frequency signal (Fig. 3) can be attributed to the alteration of sample thermal properties due to carburizing, but not

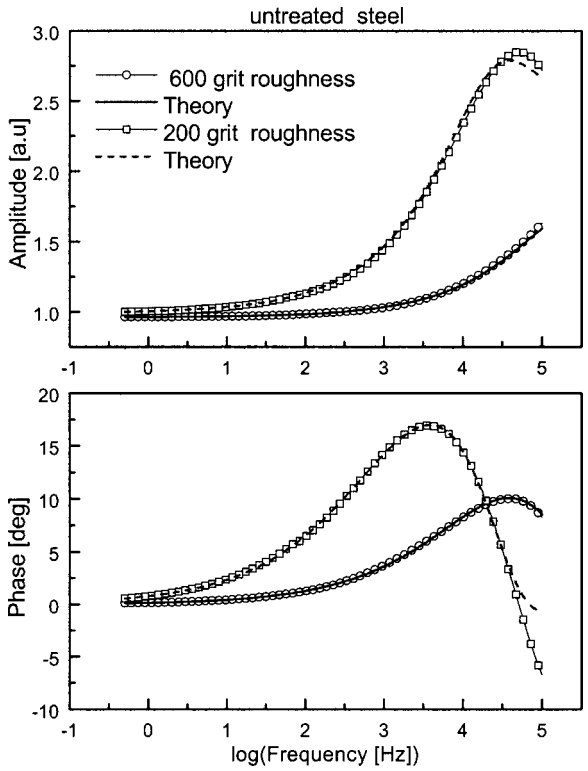

FIG. 3. Normalized experimental data for untreated samples of 600 grit (circle) and 200 grit (square) roughness. for clarity only 50% of the experimental data points are shown. Also shown are the theoretical forward fits of 600 grit (solid) and 200 grit (dashed) roughness.

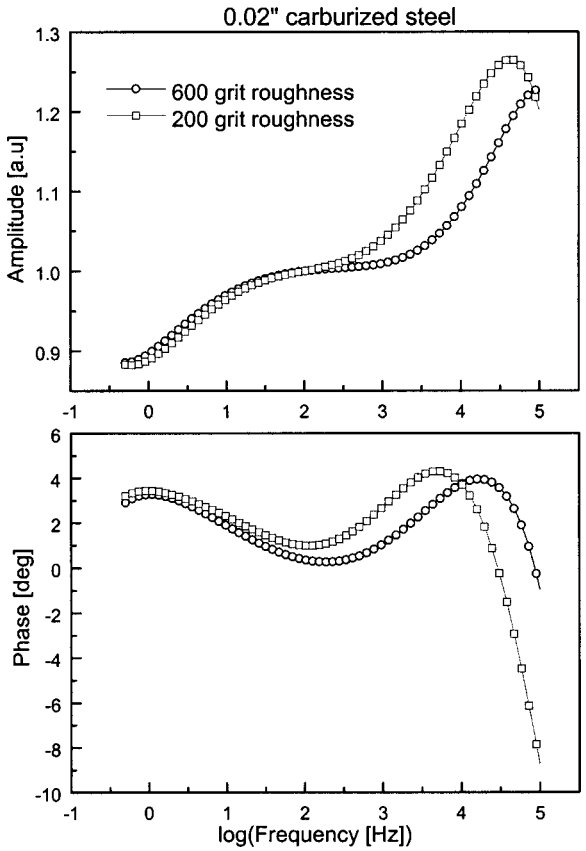

FIG. 4. Normalized experimental data of 0.02 in. carburized steel for 600 grit (circle) and 200 grit (square) roughness. For clarity only 50% of the experimental data points are shown.

to geometric changes of roughness. The full-width at half-maximum of the high frequency response peak was narrower than that of the untreated sample, indicating a change in the properties of the roughness layer. The maximum phase response at high frequency for the untreated 200 grit is $\sim 17°$ (Fig. 3) whereas after carburization the same sample has a maximum phase of $\sim 4°$ (Fig. 4). Through fitting to a theoretical formulation of an upper homogeneous layer for surface roughness, the surface thermal effusivity of these samples was found to increase (lower phase maximum) after carburizing. Furthermore, both thermal diffusivity and conductivity values of the carburized layer increased. To further investigate the effects of carburizing on the surface, the samples were studied with a scanning electron microscope (SEM). In Fig. 5, SEM pictures at X300 magnification of the surfaces (top view) are shown for the untreated (a) 600 grit, (b) 200 grit; and the carburized (c) 600 grit, (d) 200 grit samples. The SEM pictures are qualitatively consistent with the surfometer results and it is concluded that the geometrical distribution of roughness has not been significantly altered during carburization. Nevertheless, a degree of lateral fusion of the fiber-like surface structures is apparent in Figs. 5(c) and 5(d) compared to their untreated counterparts, Figs. 5(a) and 5(b), respectively.

III. THERMAL HARMONIC OSCILLATOR: TWO-LAYER APPROACH

Thermal-wave depth profilometry is a one-dimensional inverse problem where the thermal diffusivity profile is inverted from the frequency dependence of the surface temperature oscillation amplitude and phase information. Before the inverse problem can be solved, the forward problem must be developed. Our earlier depth profilometry model, built on the thermal harmonic oscillator concept,[7] treated the thermal-wave response of materials with a smoothed surface and did not account for roughness. In this work, the forward depth profilometric problem is based on formulating a one-dimensional model of a thermal-wave field from a homogeneous layer on top of a semi-infinite inhomogeneous underlayer. The inhomogeneous layer is treated via a generalization of the Hamilton–Jacobi formalism[7,8] from classical mechanics. The upper homogeneous layer has an effective adjustable thickness and thermophysical properties which are introduced into the model so as to account for the experimental frequency response in the presence of roughness on the sample (the ''underlayer''). In this manner the effects of roughness can be mathematically deconvoluted out of the total response to recover the true thermal inhomogeneities of the underlying sample.

The regions surrounding the investigated inhomogeneous layer ($x>0$) include an air–solid homogeneous interface ($x=-d$) and a solid–backing interface ($x=0$), as shown in Fig. 6. The thermal-wave fields in each region, air (a), roughness layer (1) and investigated inhomogeneous underlayer (2) are solutions to the heat conduction equation with a harmonic surface source at $x=-d$

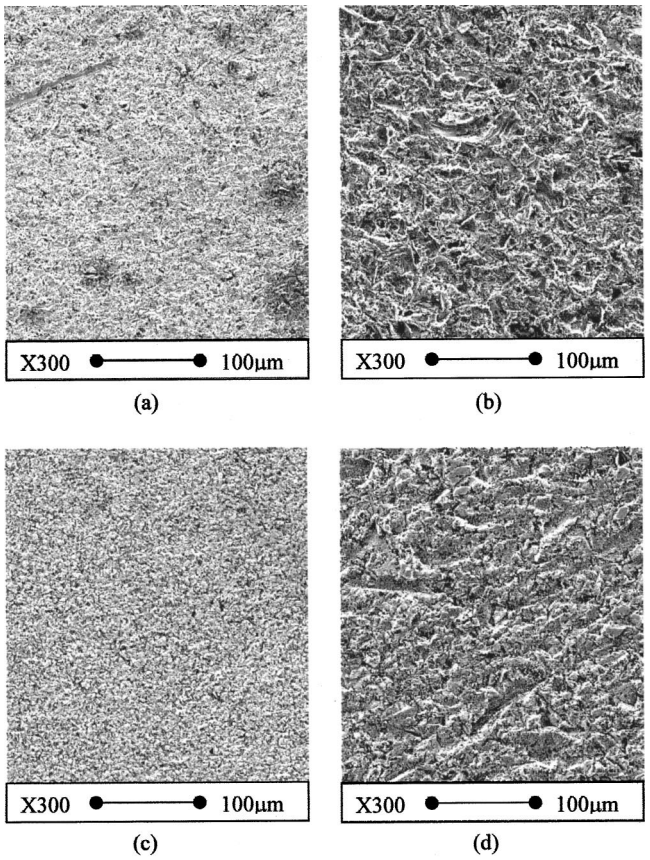

FIG. 5. Surface SEM pictures; magnification ×300; (a) untreated 600 grit roughness; (b) untreated 200 grit roughness; (c) carburized 600 grit roughness; (d) carburized 200 grit roughness.

$$T_a(x,\omega)=De^{\sigma_0(x+d)};\quad x\leqslant -d\Rightarrow x+d\leqslant 0, \tag{1}$$

$$T_1(x,\omega)=Be^{\sigma_1 x}+Ce^{-\sigma_1 x};\quad -d\leqslant x\leqslant 0, \tag{2}$$

$$T_2(x,\omega)=\frac{1}{2\sqrt{e_2(x)}}[C_1e^{H_2(x)}-C_2e^{-H_2(x)}];\quad 0\leqslant x\leqslant\infty. \tag{3}$$

Equation (1) is the bounded (finite as $x\rightarrow-\infty$) solution to the thermal-wave equation for a homogeneous semi-infinite medium and Eq. (2) is the solution for a finite homogeneous region. In Eqs. (1) and (2) σ_j is the complex wave number, defined as

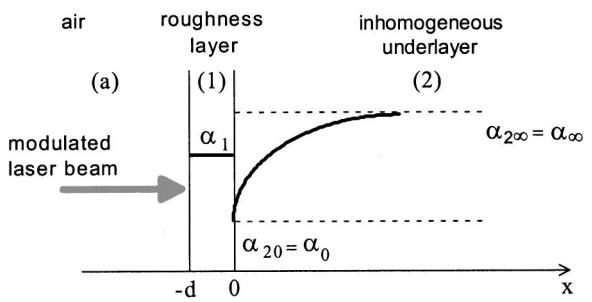

FIG. 6. Theoretical solid layer structure: (1) roughness layer; (2) inhomogeneous underlayer, the thermal diffusivity of which is to be reconstructed depth profilometrically.

$$\sigma_j(\omega)=(1+i)\sqrt{\frac{\omega}{2\alpha_j}},$$

and α_j is the thermal diffusivity of the jth medium (j:1,2). Equation (3) is the result of treating the inhomogeneous-layer thermal-wave field in terms of the Hamilton–Jacobi formulation.[7] This equation is the Wentzel–Kramers–Brillioun–Jeffreys (WKBJ) approximation of the exact solution,[8] in order to make matters more tractable computationally. The WKBJ approximation is obtained by setting the derivative of the thermal effusivity of the inhomogeneous layer equal to zero, i.e., $de_2(x)/dx=0$, where $e_2(x)=\sqrt{k_2(x)\rho_2(x)c_2(x)}$. Here $k_2(x)$ is the depth-dependent thermal conductivity, $\rho_2(x)$ is the depth-dependent density, and $c_2(x)$ is the depth-dependent specific heat at constant pressure. This assumption amounts to a requirement for non-steep local variations of the effusivity. This can always be easily satisfied, provided the thermal-wave field is evaluated at small enough depth slices by adjusting the modulation frequency increments appropriately, so that local steep diffusivity gradients may be offset.[7] It has also been shown that this approximation does not introduce error greater than a few percent in the calculation of the thermal diffusivity depth profile.[8] Constants D, B, and C depend on the boundary and limiting conditions of the system. C_1 and C_2 are integration constants and the exponent $H_2(x)$, is defined as [6]

$$H_2(x)=\int_0^x\sigma(y,\omega)dy=\int_0^x(1+i)\left(\frac{\omega}{2\alpha_2(y)}\right)^{1/2}dy, \tag{4}$$

where $\alpha_2(y)$ is the depth-dependent thermal diffusivity distribution of the solid. Solving for the constants in Eqs. (1)–(3) by using the boundary conditions of temperature and heat-flux continuity, the temperature distribution in layer (2) becomes

$$T_2(x)=\frac{Q_0\sqrt{R_2(x)}}{k_2(0)\sigma_2(0)}\left[\frac{e^{-H_2(x)}-e^{-2H_2(\infty)-H_2(x)}}{1-e^{-2H_2(\infty)}}\right]\times\left[\frac{b_{21}(0)e^{-\sigma_1 d}}{(1+b_{21}(0)F_2)-(1-b_{21}(0)F_2)e^{-2\sigma_1 d}}\right], \tag{5}$$

where Q_0 represents the thermal source fluence at the material surface [W/m^2] assuming 100% laser power absorption and

$$F_2=\frac{1+e^{-2H_2(\infty)}}{1-e^{-2H_2(\infty)}}, \tag{5a}$$

$$b_{21}(0)=\frac{k_2(0)\sigma_2(0)}{k_1\sigma_1}\equiv b_{201}, \tag{5b}$$

$$R_2(x)=\frac{e_2(0)}{e_2(x)}. \tag{5c}$$

Although it will be seen that the results are valid for arbitrary thermal diffusivity depth profiles, for this analysis the following simple simulated functional dependence of the solid inhomogeneous region thermal diffusivity is assumed[6]

$$\alpha_2(x)=\alpha_s(x)=\alpha_0\left(\frac{1+\Delta e^{-qx}}{1+\Delta}\right)^2 \tag{6}$$

such that $\alpha_s(\infty)=\alpha_\infty$, $\alpha_s(0)=\alpha_0$ and

$$\Delta=\sqrt{\frac{\alpha_0}{\alpha_\infty}}-1.$$

The parameter q is a constant that determines the rate of thermal diffusivity decay if $\alpha_0>\alpha_\infty$ or growth if $\alpha_0<\alpha_\infty$. Using Eq. (6), the resulting temperature, for the inhomogeneous layer (2) in Eq. (5), simplifies to

$$\begin{aligned}T_2(x)&=\frac{Q_0\sqrt{R_2(x)}}{k_2(0)\sigma_2(0)}\frac{b_{21}(0)e^{-\sigma_1 d-H_2(x)}}{(1+b_{21}(0))-(1-b_{21}(0))e^{-2\sigma_1 d}}\\&=\frac{Q_0\sqrt{R_2(x)}}{k_1\sigma_1}\frac{e^{-\sigma_1 d-H_2(x)}}{(1+b_{21}(0))(1-\gamma_{21}(0)e^{-2\sigma_1 d})},\end{aligned} \tag{7}$$

where

$$\gamma_{21}(0)\equiv\gamma_{201}=(1-b_{201})/(1+b_{201}). \tag{7a}$$

The superposition principle[6] is implemented in producing a complete expression for the thermal-wave field in an inhomogeneous solid bounded by the regions shown in Fig. 6. According to this principle, any complicated linear boundary-value problem can have a solution written as a linear combination of solutions to a number of simpler boundary value problems. In the case of thermal waves, the full field expression in layer (2) can be expressed as

$$T(x,\omega)=aT_2(x,\omega)+bT_0(x,\omega)+cT_\infty(x,\omega), \tag{8}$$

where T_0 and T_∞ are the thermal-wave distributions with constant thermal diffusivities a_0 and a_∞ in layer (2), respectively. They are given by

$$T_0(x,\omega)=\frac{Q_0e^{-\sigma_1 d-\sigma_{20}x}}{k_1\sigma_1(1+b_{201})(1-\gamma_{201}e^{-2\sigma_1 d})}, \tag{9a}$$

$$T_\infty(x,\omega)=\frac{Q_0e^{-\sigma_1 d-\sigma_{2\infty}x}}{k_1\sigma_1(1+b_{2\infty1})(1-\gamma_{2\infty1}e^{-2\sigma_1 d})}, \tag{9b}$$

where b_{201} and γ_{201} are as defined in Eqs. (5b) and (7a), respectively. $b_{2\infty1}$ and $\gamma_{2\infty1}$ are defined similarly by replacing 0 with ∞ in Eqs. (5b) and (7a), respectively.

Constants a, b, and c are determined by the three limiting case requirements of the problem, namely at large distance $x\to\infty$, $T(x,\omega)\to T_\infty(x,\omega)$, at very high frequency $\omega\to\infty$, $T(0,\omega)\to T_0(0,\omega)$, and at very low frequency $\omega\to0$, $T(0,\omega)\to T_\infty(0,\omega)$. Finally, substituting all the thus determined constants in Eq. (8) and calculating the field at the front surface $x=-d$ yields

$$\begin{aligned}T_1(-d,\omega)&=T(0,\omega)\frac{e^{\sigma_1 d}}{1+\gamma_{201}}(1+\gamma_{201}e^{-2\sigma_1 d})\\&=\frac{Q_0}{2k_1\sigma_1}\left[\frac{1+\gamma_{201}e^{-2\sigma_1 d}}{1-\gamma_{201}e^{-2\sigma_1 d}}\right]\\&\quad\times[1+(Z-1)e^{-\sigma_{2\infty}J_\infty}],\end{aligned} \tag{10a}$$

where

$$J_\infty=\frac{1}{2q}\ln\left(\left|\frac{\alpha_{20}}{\alpha_{2\infty}}\right|\right) \tag{10b}$$

and

$$Z=\frac{(1+b_{201})(1-\gamma_{201}e^{-2\sigma_1 d})}{(1+b_{2\infty1})(1-\gamma_{2\infty1}e^{-2\sigma_1 d})}. \tag{10c}$$

Note that the value of d cannot become unbounded ($d\to\infty$). $T(0,\omega)$ is the value of the thermal-wave field in the inhomogeneous underlayer at the interface with the effective upper (roughness) layer. Equation (10a) provides a means for studying the frequency behavior of the thermal-wave field at the surface, in terms of the integrated effect of an underlying continuously inhomogeneous semi-infinite layer on a homogeneous upper layer. The formulation of surface roughness in terms of a homogeneous upper layer is clearly a convenient approximation, the validity and limitations of which will become clear below.

IV. NUMERICAL METHOD AND THERMAL DIFFUSIVITY RECONSTRUCTIONS

Experimentally the amplitude and phase corresponding to the surface temperature distribution $T(-d,\omega)$ are obtained. The theoretical values of the data pair are calculated by

$$T(-d,\omega)=|M(\omega)|e^{i\Delta\phi(\omega)}, \tag{11}$$

where $M(\omega)$ is the thermal-wave amplitude and $\Delta\phi(\omega)$ is the phase lag at an angular frequency ω. At each frequency the amplitude and phase are used to calculate α_0 and q, introduced in Eq. (6).[9] α_∞ is needed as input and is the (assumed known) bulk thermal diffusivity. Although a diffusivity profile of the form of Eq. (6) is assumed, the actual profile is updated at each frequency by recalculating the parameters $\alpha_{0(j)}$ and q_j is a multidimensional secant method, known as Broyden's method,[6] and is based on minimizing the difference between the experimental and theoretical data for amplitude and phase as follows:

$$|M_{\exp}(\omega_j)|-|M_{\text{th}}(\omega_j)|=0, \tag{12a}$$

$$|\Delta\Phi_{\exp}(\omega_j)|-|\Delta\Phi_{\text{th}}(\omega_j)|=0. \tag{12b}$$

The calculation of the depth parameter x_j is performed based on the fact that as modulation frequency decreases the thermal-wave probing depth increases. Starting at the highest angular frequency ω_0 the shortest depth is the shortest thermal diffusion length, i.e.,

$$x_0=\sqrt{\frac{2\alpha_0}{\omega_0}}. \tag{13}$$

The next (lower) frequency, ω_{j+1} corresponds to an increased thermal-wave depth

$$x_{j+1}=x_j+\sqrt{\frac{2\alpha_j}{\omega_{j+1}}}-\sqrt{\frac{2\alpha_j}{\omega_j}}, \tag{14}$$

which is used to calculate α_{j+1} in Eq. (6). Once the α_{j+1} is calculated, the method returns to calculate in recursive iteration the increased thermal-wave depth as

$$x_{j+1}=x_j+\sqrt{\frac{2\alpha_{j+1}}{\omega_{j+1}}}-\sqrt{\frac{2\alpha_j}{\omega_j}}. \tag{15}$$

In reconstructing depth profiles from data it is important to first find a reliable set of initial values for α_0 and q. This may be achieved by finding the best forward theoretical fit to the first few end points (high frequency) using a single profile of the form of Eq. (6).[9] With knowledge of the bulk thermal diffusivity and the thickness of the surface roughness (600 and 200 grit) of the untreated AISI 8620 steel samples, a reconstruction can be performed. The bulk thermal diffusivity was measured independently and was found to be $\alpha_\infty=12.5\times10^{-6}$ m^2/s. The inversion is based on reconstructing from the high frequency end by fitting the α_0 at the interface with the geometry shown in Fig. 6. With this method the effect of surface roughness is greatly reduced from the system. For the 600 grit roughness sample the input parameters were $\alpha_d=4.5\times10^{-6}$ m^2/s, $k_d=10.1$ W/mK ($e_d=4.67\times10^3$ $Ws^{1/2}/m^2K$) and roughness thickness $d=2.5$ μm. Here, α_d and k_d stand for the mean thermal diffusivity and conductivity of the rough layer, respectively. For the 200 grit roughness sample the input parameters were $\alpha_d=2.2\times10^{-6}$ m^2/s, $k_d=4.6$ W/mK ($e_d=3.1\times10^3$ $Ws^{1/2}/m^2K$) and roughness thickness $d=5$ μm. It is observed that as roughness increases the effective thermal effusivity of the surface layer ($x<-d$) decreases. Qualitatively, this can be understood phenomenologically by considering that roughness consists ideally of a series of pyramidal (or conical or triangular fin-like) structures of decreasing spatial extent away from the baseline.[10] For a given modulation frequency, the laser-generated thermal wave penetrates deeper into the continuous substrate in the case of the smoother surface (600 grit roughness) than in the case of the rougher surface. Therefore, the contribution of the better thermophysical properties of the substrate to the depth-weighed mean values diffusivity and conductivity in the former case is proportionately more substantial than in the latter case. This results in the higher overall mean thermal properties of the smoother surface measured through photothermal radiometry. In both cases the mean thermal diffusion lengths around the peaks of the maximum roughness effects in Fig. 3 were approximately 12 μm. This penetration depth is consistent with a strong thermal communication with, and thermophysical contribution from, the substrate for both roughness thicknesses. The forward theoretical fits to the untreated experimental data that assume an optimally adjusted homogeneous layer on a semi-infinite homogeneous substrate (represented by the untreated steel) are shown in Fig. 3. Similar forward theoretical fits were applied to the high-frequency peaks of the carburized steel, Fig. 4. The resulting thermophysical values of the effective roughness layer were: For the 600 grit roughness sample $\alpha_d=2.3\times10^{-6}$ m^2/s and $k_d=9.8$ W/mK. For the 200 grit sample, $\alpha_d=2.5\times10^{-6}$ m^2/s and $k_d=10.25$ W/mK. Comparison of the $d=5$ μm roughness, 200 grit samples, before and after carburization shows an increase in the (α_d,k_d) values, perhaps the result of the lateral connectivity of surface structures, Figs. 5(b) and 5(d). This would tend to enhance thermal diffusion across previously isolated ''islands'' (fiber bundles). The decrease in (α_d,k_d) values of the $d=2.5$ mm roughness layer is probably an artifact of the decreased substrate near-surface diffusivity following carburization (see Fig. 13), coupled with the greater contribution of substrate thermophysical properties to the mean thermal diffusion length of the rough layer in the 600 grit sample. Overall the forward theoretical fit is in excellent agreement with the experimental data over a wide frequency range. Nevertheless, small discrepancies exist at the high frequency end, where roughness is more difficult to model as a uniform layer. A reconstruction for the untreated AISI 8620 samples with the method outlined above was performed. The experimental data were numerically inverted to obtain the corresponding thermal diffusivity profiles, as shown in Fig. 7. The rough layer, which was assumed to be homogeneous with low thermal parameters, was theoretically eliminated. Thus, the reconstruction shown in Fig. 7 commences below the rough layer. It is seen that the reconstruction based on the uniform overlayer concept is unable to fully eliminate surface roughness. As a result, the thermophysical properties of the underlayer exhibit nonuniformity artifacts down to about 50 and 600 μm for the 600 and 200 grit roughness, respectively. Below these depths the depth profile reconstruction is adequate: The thermal diffusivity of the bulk material remains flat and approaches the independently measured value of $\alpha_\infty=12.5\times10^{-6}$ m^2/s for both samples. Besides the approximate modeling of roughness as a homogeneous layer, the near-surface profile can also be attributed to the violation of the WKBJ approximation, Eq. (3), at high frequencies, where much finer Δf increments may be required in order to satisfy the nonsteep local thermal effusivity variation condition for the validity of that equation. For low-roughness materials, the near-surface inadequacy of the homogeneous overlayer model of Fig. 7 can be neglected, since hardness measurements are usually of interest deeper than 50 μm. In any case, such a reconstruction can serve as a guide to determine the extent to which roughness influences a specific profile. As roughness size increases, the reconstruction becomes less reliable. There are two reasons for this; (1) the

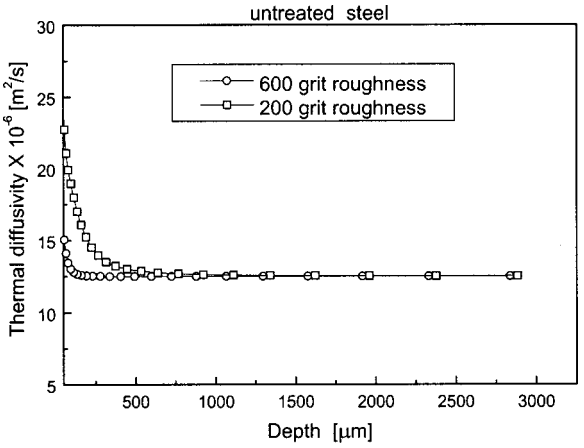

FIG. 7. Reconstruction of experimental 600 grit (circle) and 200 grit (square) untreated samples.

forward model is inadequate at the high-end frequency spectrum where the nonuniformity (randomness) of roughness is more evident; and (2) the inverse problem becomes more ill posed, since more variables (effective roughness properties) are introduced. In conclusion, thermal diffusivity reconstructions under a uniform overlayer assumption based on Eq. (16) are quite straightforward and simple enough, but can only be satisfactory for materials with thin roughness overlayers.

V. THEORETICAL MODEL OF ROUGHNESS: LOGARITHMIC-GAUSSIAN MODEL APPROACH

A. Roughness elimination method

The foregoing theoretical model of treating roughness as a homogeneous layer over an inhomogeneous substrate, albeit quite successful with thin roughness layers, it is, however, too simplistic. Using a flat (homogeneous) underlayer it was seen, Fig. 7, that as the level (thickness) of roughness increases the thermal-wave spectrum cannot be adequately interpreted by an effective uniform overlayer, resulting in an erroneous thermal diffusivity profile. In a frequency domain method both roughness and underlayer inhomogeneities are observed throughout the frequency spectrum. An approach based on linear superposition of several uniform overlayers[1] for deconvolving roughness inhomogeneity from that of the substrate might not be generally valid, since the roughness-generated frequency response is often nonlinear. Therefore, an approach is adopted and tested for various levels of roughness and substrate inhomogeneity. The idea behind this roughness elimination method is based on recognizing distinct features (phase maxima) in the frequency spectrum. Since roughness is associated with the surface of a sample, the effects are strongest at high frequencies, whereas the low frequency end is mostly associated with substrate inhomogeneities. Again, the objective of the method is to deconvolve out the roughness spectrum and reveal the desirable underlying thermal diffusivity depth profile (homogeneous or inhomogeneous).

To demonstrate how roughness is eliminated from the total field, three simulations of increasing roughness with the same inhomogeneous profile (developed in the theoretical model of Sec. III) were performed, with the upper layer being rough. Case A is illustrated in Fig. 8 for a roughness thickness $d=1.6$ μm. Curve 1 shows the theoretical response of a semi-infinite *inhomogeneous* sample with roughness, the latter modeled as an effective *homogeneous* upper layer. Curve 2 represents the theoretical response of the same semi-infinite *inhomogeneous* sample without roughness. Curve 3 is a simulated *homogeneous* layer with thermal diffusivity value equal to that of the back surface of the underlayer considered in curve 2 with roughness. The objective of the method is to retrieve curve 2 from curve 1 by means of eliminating roughness. Curve 4 is a theoretical fit to the high-frequency end of curve 1 (the region associated with roughness), using the theory for a semi-infinite homogeneous substrate with roughness. The input parameters of curve 4 are the same as the ones used for curve 3, except that an effective thermal conductivity is used for the roughness layer to match the high-frequency end of curve 1. The parameters used to obtain case A, curves 1–4 are shown in Table I. Using a simple normalization procedure of the total field, curves 1 and 4 yield

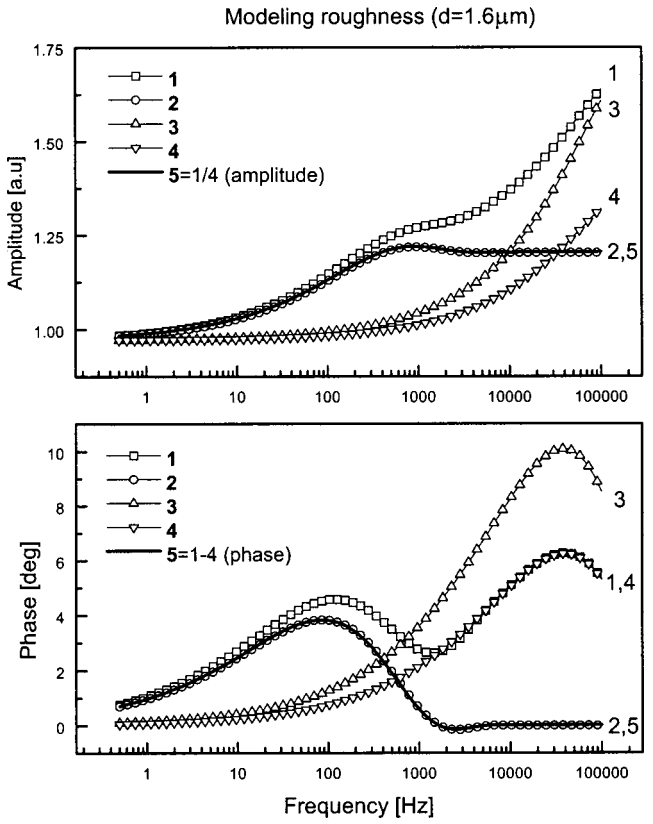

FIG. 8. Simulation of roughness elimination method with 1.6 μm roughness thickness. Curve 1 (square): inhomogeneous with roughness; curve 2 (circle): inhomogeneous with no roughness; curve 3 (upward triangle): homogeneous with roughness; curve 4 (downward triangle): effective homogeneous with roughness; curve 5 (solid): normalized inhomogeneous with no roughness.

TABLE I. Thermal properties of simulations for cases A, B, and C.

Thermal properties	Case A	Case B	Case C
	$d=1.6$ μm	$d=7$ μm	$d=13$ μm
	$\alpha_\infty=6.15\times10^{-6}$ m^2/s		
curve 1:	$\alpha_0=4.0\times10^{-6}$ m^2/s		
total field:	$q=2\times10^3$ m^{-1}		
inhomogeneous	$\alpha_d=2.1\times10^{-6}$ m^2/s		
with roughness	$k_d=4.8$ W/mK		
	$\alpha_\infty=6.15\times10^{-6}$ m^2/s		
curve 2	$\alpha_0=4.0\times10^{-6}$ m^2/s		
inhomogeneous	$q=2\times10^3$ m^{-1}		
with no roughness	$d=0$ μm		
	$\alpha_\infty=6.15\times10^{-6}$ m^2/s		
curve 3:	$\alpha_0=6.15\times10^{-6}$ m^2/s		
homogeneous	$\alpha_d=2.1\times10^{-6}$ m^2/s		
with roughness	$k_d=4.8$ W/mK		
curve 4:	$\alpha_\infty=6.15\times10^{-6}$ m^2/s		
homogeneous with	$\alpha_0=6.15\times10^{-6}$ m^2/s		
effective roughness	$\alpha_d=2.1\times10^{-6}$ m^2/s		
	$k_{d(\text{eff})}=5.96$ W/mK		

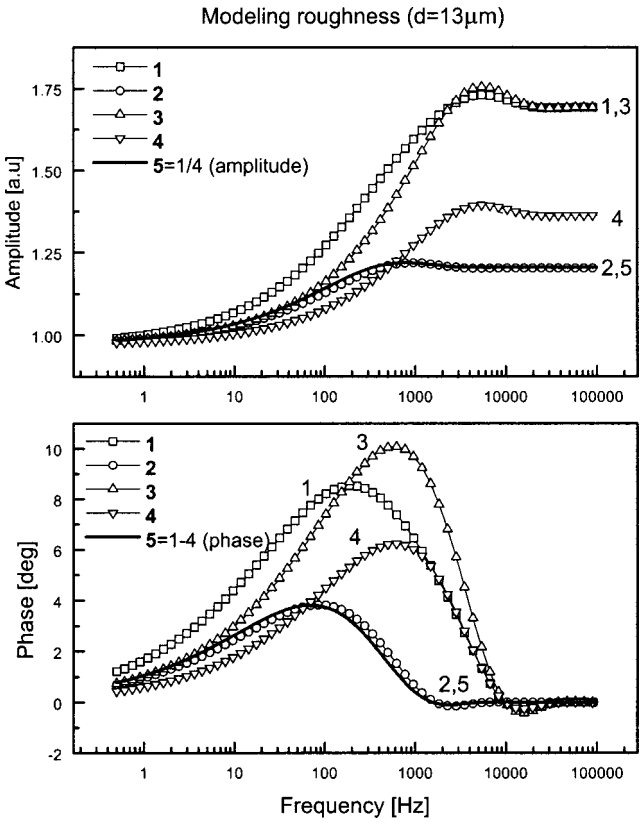

FIG. 9. Simulation of roughness elimination method with 13 μm roughness thickness. Curve 1 (square): inhomogeneous with roughness; curve 2 (circle): inhomogeneous with no roughness; curve 3 (upward triangle): homogeneous with roughness; curve 4 (downward triangle): effective homogeneous with roughness; curve 5 (solid): normalized inhomogeneous with no roughness.

$$T_{\text{final}(5)}(0,\omega)=\frac{\text{Curve } 1}{\text{Curve } 4}=\frac{|M_{\text{total}}(\omega)|e^{i\Delta\Phi_{\text{total}}\omega)}}{|M_{\text{eff}}(\omega)|e^{i\Delta\Phi_{\text{eff}}(\omega)}}, \tag{16}$$

which is plotted as curve 5. Comparing the result with the original *inhomogeneous* response with no roughness (curve 2), excellent agreement is evident. Therefore, it is seen that the result of the mathematical operation, (inhomogeneous layer+roughness)*(homogeneous layer+roughness) =inhomogeneous layer, eliminates roughness while preserving the effects of the thermophysical inhomogeneity. Here * stands for the ratioing or subtraction operation associated with the amplitude or phase normalization of Eq. (16).

The method was further tested successfully with a higher scale of roughness (case B in Table I), with $d=7$ μm. Here, the amplitude and phase exhibit characteristic maxima as in case A. The thermophysical values for each curve are the same as those of case A. A more complicated situation involving a thicker roughness layer with $d=13$ μm, case C, was then examined. In this case the spectral features due to roughness almost fully overlap those due to underlayer inhomogeneities. Neither the amplitude nor the phase shows any characteristic maxima from which roughness alone can be inferred (Fig. 9). The extrema in Fig. 9 are due to roughness and inhomogeneities together. The results of prior simulations (cases A and B) showed that the same inhomogeneities affect the frequency spectrum in a similar manner. Thus, curve 4 for case C was constructed using the same effective properties as in case A with the only difference being the roughness thickness d. The thermophysical values used in case C are the same as in the other cases. For this case, the deviations of curve 5 from the theoretical value of curve 2 are more pronounced as compared to cases A and B, but are still within very satisfactory boundaries. Therefore, the use of a reference solid with small enough roughness with distinct phase maxima for inhomogeneity and roughness can assist in retrieving the inhomogeneity of a rougher sample with no separation between roughness and inhomogeneity. In conclusion, the foregoing numerical examples show that it is possible to eliminate surface roughness from thermal-wave spectra for a wide range of roughness thicknesses.

B. Logarithmic-Gaussian roughness modeling

A general expression not based on knowledge of the thermophysical properties of roughness is now sought, so as to yield an appropriate roughness model. This model can then be used to eliminate roughness from the total field using the method of Sec. V A, without having to use uniform overlayer models and the concomitant limitations. By invoking the concept that random roughness is equivalent to a Gaussian distribution in the spatial depth coordinate, i.e., it corresponds to spatial white noise, the effects of inhomogeneity and roughness can be deconvoluted. For this reason a logarithmic-Gaussian noise profile is fitted to the effective frequency-domain roughness distribution based on the theoretically expected Gaussian-to-Gaussian Fourier transformation between the spatial coordinate and the spatial frequency, which, in turn, depends on the modulation frequency through the local thermal diffusion coefficient. The roughness spatial Gaussian profile is thus mapped as a Gaussian distribution in the log-frequency coordinate. By extension, a linear superposition of several such Gaussian functions can be conceived if there are multiple characteristic roughness scales associated with a particular rough surface as pictorially illustrated in Fig. 2 for the case of two such scales. The superposition spatial-frequency field thus created is nonsymmetric and the expressions for amplitude and phase, respectively, are as follows:

$$M_{\text{eff}}(\omega_0)=M_0+\sqrt{\frac{2}{\pi}}\sum_{i=2}^{N}\frac{A_{1i}}{\log(W_{1i})}\times e^{-[(\log(\omega_{10})-\log(\omega_{1ci}))^2/(\log(W_{1i}))]}, \tag{17}$$

$$\Delta\Phi_{\text{eff}}(\omega_0)=\Delta\Phi_0+\sqrt{\frac{2}{\pi}}\sum_{i=2}^{N}\frac{A_{2i}}{\log(W_{2i})}\times e^{-[(\log(\omega_{20})-\log(\omega_{2ci}))^2/(\log(W_{2i}))]}. \tag{18}$$

where $\log(W)$ is the e^{-2} width of the spatial-frequency logarithmic-Gaussian distribution, A is the area under the line shape, and ω_c is the angular frequency at line center of the Gaussian function. N is the maximum number of characteristic roughness lengths anticipated. The summation of Gaussians is greater than one ($N>1$) so as to account for the asymmetry of the field. Physically this denotes that there is no possibility of a single roughness scale at least for our

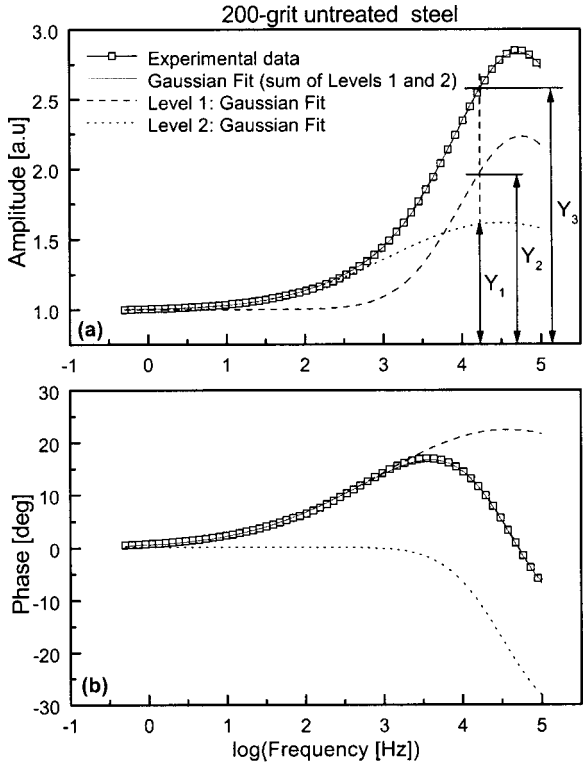

FIG. 10. Logarithmic-Gaussian fit (solid line) to the roughness spectrum of the untreated 200 grit roughness experimental data (squares). Dashed line: logarithmic-Gaussian fit associated with scale 1 roughness; Dotted line: logarithmic-Gaussian fit associated with scale 2 roughness. Y_1 and Y_2: amplitude components of the linear Gaussian superposition, Eq. (17).

experiments. Perhaps, the complexity of the roughness layers encountered in this work is such that at best they can be modeled with two scales as seen in Fig. 2. M_0 and $\Delta\Phi_0$ are the amplitude and phase offset, respectively. These offset values represent the signal value (saturation) at which the roughness will no longer distort the phothermal signal. The approximate offset values at low frequencies ($f<1$ Hz) are ''1'' for amplitude and ''0'' for phase. These values represent the normalized homogeneous response to the reference Zr alloy without roughness. Hence, in order to retrieve and eliminate roughness from the experimental data, a logarithmic-Gaussian fit to the high frequency end is made based on Eqs. (17) and (18). When fitting the summation of logarithmic-Gaussians to a given roughness profile each Gaussian function is associated with a different log-frequency constant. This is physically reasonable if roughness is viewed as several spatial white-noise levels (''scales''), each level belonging to a characteristic-length-scale parameter (a roughness band or strip). A random spatial (''white-noise'') roughness distribution exists about each characteristic value belonging to a particular scale. Each scale of roughness is thus described by a characteristic frequency range, mapped into a particular logarithmic-Gaussian distribution. The logarithmic-Gaussian distribution is derived from the Central Limit Theorem in cases when random variables in the distribution are not independent.[11] It may thus be argued that the roughness scales are not truly mutually independent and are normally distributed, in the Gaussian sense, along the log(f) axis. Figure 10, illustrates the logarithmic-Gaussian distribution (solid line) for the untreated 200 grit roughness sample. The individual logarithmic Gaussians associated with each roughness scale are also shown with the values documented in Table II. For this roughness profile it is found that there are two characteristic-length parameters (double logarithmic Gaussian). Given that the double distribution fit in Fig. 10(a) requires each amplitude component Y_1 and Y_2 to satisfy a Gaussian profile at each frequency, and that the algebraic sum of each pair of points (Y_1+Y_2) must be equal to a fixed number y_3, determined by the data, it was empirically found that the combination of components (Y_1,Y_2) is unique. Therefore, the two amplitude characteristic-length parameters are also unique. Similar results are found with respect to phase, Fig. 10(b), of the untreated sample, as well as for the treated sample, Fig. 11.

TABLE II. Gaussian fit parameters to the untreated and 0.02 in. carburized 200 grit roughness samples. ω_{ci} represent characteristic angular frequencies of roughness scale $i(=1,2,3)$.

Gaussian fit	Untreated 600 grit roughness		Carburized 200 grit roughness	
	amplitude	phase	amplitude	phase
M_0 or $\Delta\Phi_0$	1	0.11	0.98	0.11
$\log(\omega_{c1})$	4.75	4.57	4.81	4.96
$\log(W_1)$	1.53	3.29	0.81	2.28
A_1	2.36	91.79	0.12	41.86
$\log(\omega_{c2})$	4.48	5.26	4.34	5.81
$\log(W_2)$	2.83	1.45	1.32	3.02
A_2	2.18	−54.74	0.29	−82.02
$\log(\omega_{c3})$	⋯	⋯	3.38	⋯
$\log(W_3)$	⋯	⋯	2.47	⋯
A_3	⋯	⋯	0.13	⋯

C. Application to carburized steels

Figure 11 shows the fitted logarithmic-Gaussian distribution to the carburized experimental data with 200 grit roughness. The profile needed to perform such an operation on these data is a summation of logarithmic Gaussians whose parameters can be found in Table II. Although the phase roughness is fitted well to a double logarithmic-Gaussian function, the amplitude requires a summation of three logarithmic Gaussians to account for the experimental behavior at the high-frequency end of the spectrum. Figure 12 shows the experimental data for the carburized samples with 600 and 200 grit roughness after the elimination of roughness. Despite two different roughness profiles, the same inhomogeneous underlayer experimental response is revealed. The experimental data were then used for thermal diffusivity reconstructions, with the computational methodology developed in Sec. IV assuming no roughness ($d=0$). The reconstructed depth profiles of the hardened samples exhibited an anticorrelation between thermal diffusivity and hardness, Fig. 13, which is consistent with earlier reports.[10,12]

An important aspect of the reconstruction procedure is the understanding of the physical mechanism for the anticorrelation between thermal diffusivity and hardness. Current techniques have not separately addressed the effects of different heat treatments on the thermal diffusivity profile of

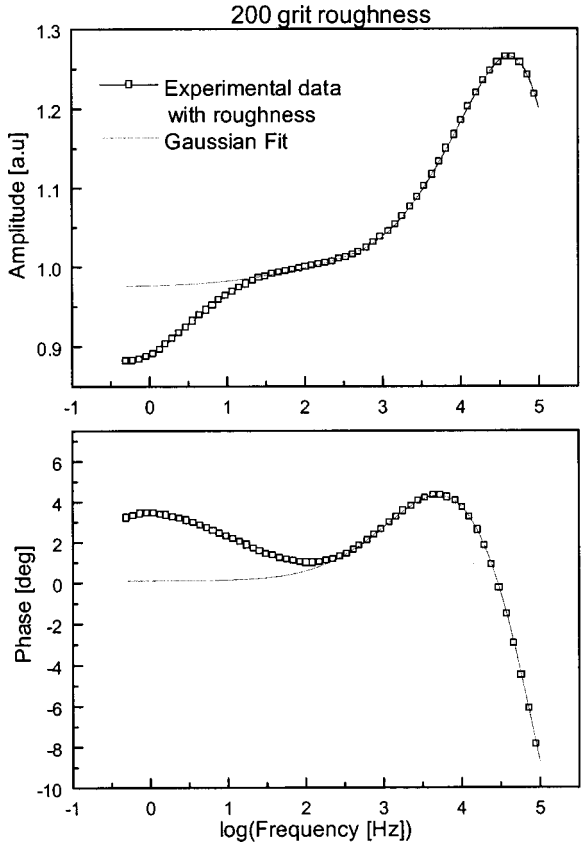

FIG. 11. Logarithmic-Gaussian fit (solid line) to the roughness spectrum of the carburized 200 grit roughness experimental data (squares).

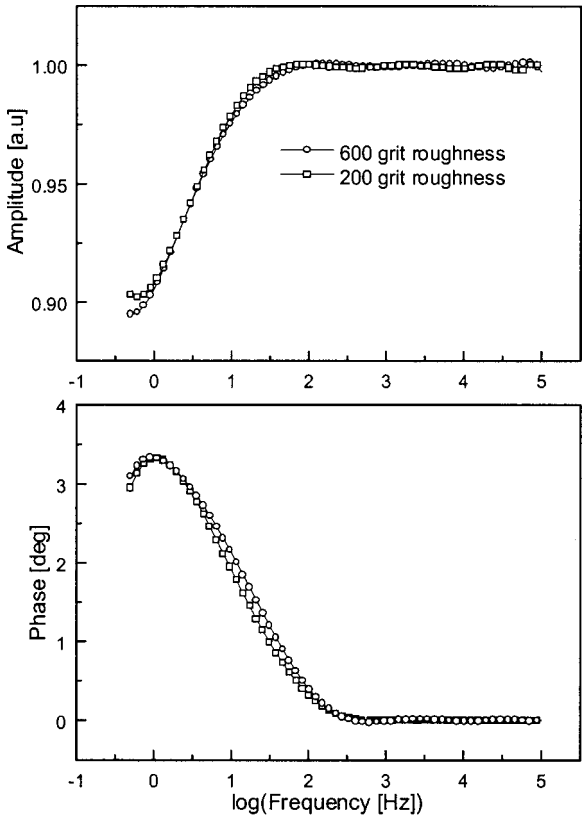

FIG. 12. Carburized experimental data after elimination of roughness for 0.02 in case depth with 600 grit (circles) and 200 grit (squares) roughness.

steels. Therefore, the exact nature of the anticorrelation between thermal diffusivity and microhardness has not been properly understood. A very recent detailed study focused on finding the mechanism of the anticorrelation has been reported,[13] which concluded that the carbon diffusion profile during heat treatment controls the thermal diffusivity depth profile of carburized AISI 8620 steels. Further depth profilometric studies using different grades of steels are currently under way.

VI. CONCLUSIONS

Two approaches for treating surface roughness on the surface of inhomogeneous solids have been introduced. One approach consists of an effective homogeneous overlayer with thickness and thermophysical properties adjusted to fit high-frequency experimental thermal-wave data. This method was shown to yield good deconvolution and mathematical elimination of roughness only in the limit of thin roughness layers. Another, more broadly valid approach models roughness as spatial white noise. This method leads to a linear superposition of Gaussian roughness profile scales in the log-frequency domain (logarithmic Gaussian). It has helped establish a procedure for eliminating the effects of a roughness layer of arbitrary thickness from the frequency response of the inhomogeneous substrate. The logarithmic-Gaussian elimination of roughness proves to be an effective method for use with wide roughness scales, revealing the ''true'' thermal-wave frequency response of underlayers from experimental data convoluted with the roughness spectrum. In this manner, reliable thermal diffusivity reconstructions of inhomogeneous underlayers from experimental laser infrared photothermal radiometric data from AISI 8620 steels have been achieved. The Gaussian method further provides physical insight into the effective thermal structure of rough surfaces through their frequency response under the thermal-wave probe. It has the advantage over other roughness methods[1] of not requiring specific structural assumptions regarding the geometry of the rough layer.

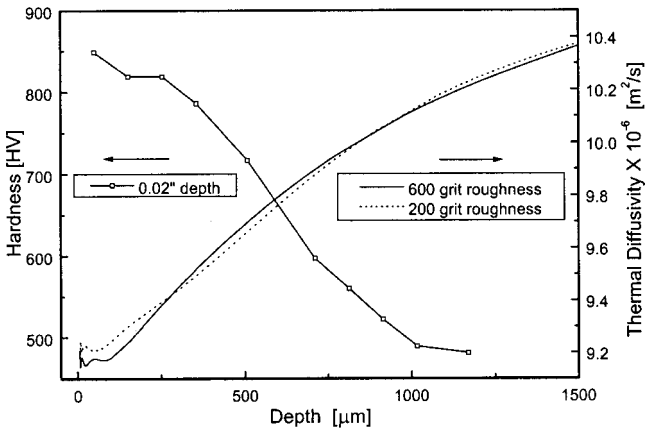

FIG. 13. Hardness and thermal diffusivity profile reconstructions for 0.02 in case-depth carburized data with 600 grit (solid line) and 200 grit (dashed line) roughness.

ACKNOWLEDGMENT

The support of Materials and Manufacturing Ontario (MMO) is gratefully acknowledged.

[1] B. K. Bein, S. Krueger, and J. Pelzl, Can. J. Phys. **64**, 1208 (1986); B. K. Bein, J. H. Gu, A. Mensing, T. Sommer, B. Wuderlich, J. Pelzl, and U. Seidel, Mater. Eval. **45**, 471 (1987).
[2] R. Osiander, R. Haberken, P. Korpium, and W. Schirmacher, in *Photoacoustic and Photothermal Phenomena II*, edited by J. C. Murphy, J. W. Maclachlan-Spicer, L. Aamodt, and B. S. H. Royce (Springer, Berlin, 1990), Vol. 62, p. 309.
[3] S. Alexander and R. Orbach, J. Phys. (France) Lett. **43**, L625 (1982).
[4] A. C. Boccara and D. Fournier, in *Photoacoustic and Thermal Wave Phenomena in Semiconductors*, edited by A. Mandelis (Elsevier, New York, 1987), p. 308; A. C. Boccara and D. Fournier, in *Photoacoustic and Photothermal Phenomena*, edited by P. Hess and J. Pelzl (Springer, Berlin, 1988); D. Fournier and A. C. Boccara, Physica **157**, 587 (1989).
[5] D. Vandembroucq and S. Roux, Phys. Rev. E **55**, 6171 (1997); **55**, 6186 (1997); D. Vandembroucq and A. C. Boccara, Prog. Nat. Sci. **6**, S-321 (1996).
[6] A. Mandelis, F. Funak, and M. Munidasa, J. Appl. Phys. **80**, 5570 (1996).
[7] A. Mandelis, J. Math. Phys. **26**, 2676 (1985).
[8] A. Mandelis, S. B. Peralta, and J. Thoen, J. Appl. Phys. **70**, 1761 (1991); A. Mandelis, E. Schoubs, S. B. Peralta, and J. Thoen, *ibid.* **70**, 1771 (1991).
[9] M. Munidasa, F. Funak, and A. Mandelis, J. Appl. Phys. **83**, 3495 (1998).
[10] W. Kiepert, B. K. Bein, J. H. Gu, J. Pelzl, and H. G. Walther, in *Progress in Natural Science Suppl. Vol. 6*, edited by S.-Y. Zhang (Taylor and Francis, Beijing, 1999), p. S-317.
[11] H. Cramer, *Mathematical Methods of Statistics* (Princeton University Press, Princeton, NJ, 1946).
[12] T. T. N. Lan, U. Seidel, H. G. Walther, G. Goch, and B. Schmitz, J. Appl. Phys. **78**, 4108 (1995).
[13] L. Nicolaides, A. Mandelis, and C. J. Beingessner, J. Appl. Phys. (in press).